SLAC-PUB-16222

Exploring Mbar shock conditions and isochorically heated aluminum at the MEC end station of the LCLS[b.)]

L. B. Fletcher[1,2], H. J. Lee[1], B. Barbrel[2], M. Gauthier[1], E. Galtier[1], B. Nagler[1], T. Döppner[3], S. LePape[3], T. Ma[3], A. Pak[3], D. Turnbull[3], T. White[4], G. Gregori[4], M. Wei[5], R. W. Falcone[2], P. Heimann[1], U. Zastrau[1,6], J. B. Hastings[1] and S. H. Glenzer[1]

[1]*SLAC National Accelerator Laboratory, 2575 Sand Hill Road, Menlo Park, CA, 94025, USA*
[2]*Physics Department, University of California Berkeley, Berkeley, CA, 94709, USA*
[3]*Lawrence Livermore National Laboratory, P.O. Box 808, Livermore, CA, 94551, USA*
[4]*University of Oxford, Parks Road, Oxford, OX1 3PU, UK*
[5]*General Atomics, San Diego, CA, 87544, USA*
[6]*Institute for Optics and Quantum Electronics, Friedrich-Schiller-University, 07743 Jena, Germany*

Recent experiments performed at the Matter in Extreme Conditions end station (MEC) of the Linac Coherent Light Source (LCLS) have demonstrated the first spectrally resolved measurements of plasmons from isochorically heated aluminum. The experiments have been performed using a seeded 8-keV x-ray laser beam as a pump and probe to both volumetrically heat and scatter x-rays from aluminum. Collective x-ray Thomson scattering spectra show a well-resolved plasmon feature that is down-shifted in energy by 19 eV. In addition, Mbar shock pressures from laser-compressed aluminum foils using Velocity Interferometer System for Any Reflector (VISAR) have been measured. The combination of experiments fully demonstrates the possibility to perform warm dense matter studies at the LCLS with unprecedented accuracy and precision.

I. INTRODUCTION

Spectrally resolved x-ray scattering can be used as a novel probing technique to directly measure dense plasma conditions of compressed solids at mega bar pressures. The ultrafast time resolution provided by the LCLS x-ray source allows for studies of high-pressure phase transitions [1,2], observations of novel structural properties [3], or direct measurements of material strain rates. Moreover, knowledge of dense plasma conditions are important for warm dense matter studies and potential applications related to particle acceleration [4,5], inertial confinement fusion [6,7], and laboratory astrophysics [8,9].

Unprecedented experimental capabilities have recently become available to accurately explore extreme matter conditions [10] with both the LCLS x-ray laser [11] and the commissioning of the MEC end station. The MEC end station is equipped with two nanosecond laser beams, at 2.5 GW, that can drive material into extreme matter conditions by launching shock waves that propagate through solid targets. Under these conditions, spectrally resolved x-ray Thomson scattering measurements in the non-collective (backward) scattering regime can provide information of the microscopic physics by measuring the free electron distribution function. In addition, measurements in the forward scattering regime, collective electron oscillations (plasmons) [12-14] can simultaneously be observed. The plasmon scattering spectrum is of fundamental interest because it holds promise to determine plasma parameters and the physical properties from first principles [15]. This is particularly relevant for plasmas at and above solid density where the material is often strongly coupled and standard theoretical approximations that have been developed for solids, or ideal plasmas, are not applicable. Previous x-ray Thomson scattering studies that use laser-generated x-ray sources in the collective regime have often been insufficient to resolve plasmon signals in low-density plasmas due to the large bandwidth of the input source spectrum [16].

The LCLS beam, in seeded mode operation, delivers approximately 10^{12} x-ray photons in a micron-scale focal spot allowing measurements with high spectral resolution of $\Delta E/E = 10^{-4}$, high wave-number resolution of $\Delta k/k = 10^{-2}$, and high temporal resolution of 20-50 fs. Consequently, by employing highly efficient curved crystal spectrometers, the plasmon spectrum can be observed and resolved in a single x-ray pulse. Experiments have been performed in both a single shot mode and a high repetition rate mode of 120 Hz. The latter allows for measurements of quasi noise-free plasmon spectra within 7 seconds that determine the plasmon dispersion and intensity for warm solid-density aluminum. A plasmon shift of 19 eV yields $n_e = 1.8 \times 10^{23}$ cm^{-3}, expected for Z = 3 and temperatures less than 0.1 eV. These findings [17] demonstrate the plasmon scattering capability at LCLS and will motivate future investigations in hot compressed matter.

In addition to the spectrally resolved capabilities, the MEC end station offers the ability to operate parallel VISAR measurements to fully characterize laser-drive conditions, monitor shock propagation, as well as serve as a platform to evaluate equation of state (EOS) models of materials under extreme conditions. We will demonstrate in this study, using VISAR measurements, the ability to produce 20 μm diameter

[b)] Invited paper published as part of the Proceedings of the 20th Topical Conference on High-Temperature Plasma Diagnostics, Atlanta, Georgia, June, 2014.

This material is based upon work supported by the U.S. Department of Energy, Office of Science, Office of Basic Energy Sciences, under Contract No. DE-AC02-76SF00515 and FES.

planar shocks above 1 Mbar to a depth of 25 μm in CH coated aluminum foils using laser intensities of 35 TW/cm^2.

A. Spectrally resolved X-ray Thomson scattering

X-ray Thomson scattering has proven to be an accurate diagnostic tool that can be used to determine the properties of dense plasmas [3,7]. The scattered cross section Eq. (1) can be described in terms of the Thomson scattering cross-section σ_T, k_1 and k_o, the scattered and incident wave vectors, respectively, and the total dynamic electron structure factor S(k,ω):

$$\frac{\partial^2 \sigma_T}{\partial \Omega \partial \omega} = \sigma_T \frac{k_1}{k_0} S(k,\omega) \tag{1}$$

It is possible to separate the total density fluctuations included in the structure factor between the free Z_f and bound Z_b electron contributions, as well as electrons following the motion of the ions. The total dynamic electron structure factor [18-20], S(k,ω), can be described by:

$$\begin{aligned} S(k,\omega) &= \left|f_1(k)+q(k)\right|^2 S_{ii}(k,\omega) + Z_f S^o_{ee}(k,\omega) \\ &\quad \ldots \\ &\quad + Z_b \int S_{ce}(k,\omega-\omega') S_s(k,\omega') \partial\omega' \end{aligned} \tag{2}$$

The first term in Eq. (2) results from elastic scattering of tightly bound electrons (Rayleigh scatter) that are co-moving with the ions where $f_1(k)$ is the atomic form factor describing the elastic scattering from bound electrons, q(k) contains the contribution from the electrons in the screening cloud around the ion, and $S_{ii}(k,\omega)$ is the ion-ion density correlation function. The second term in Eq. (2) describes the inelastic scattering due to free electrons, where $S^0_{ee}(k,\omega)$ is the free electron-electron density correlation function and Z_f is the effective ionization state. The third term in Eq. (2) describes inelastic excitations of bound states within an atom or ion into the continuum, represented by $S_{ce}(k,\omega)$ where Z_b=Z-Z_f.

The magnitude of the k-vector can be given by:

$$k = |\mathrm{k}| = \frac{4\pi hc}{E_0} \sin\left(\frac{\theta}{2}\right) \tag{3}$$

with $E_0 = h\omega_0/2\pi$ being the energy of the probe x rays and θ the scattering angle. Momentum and energy are transferred to free electrons and to the electrons with binding energy less than $h\omega_C/2\pi$. With the scattering vector defined by x-ray energy and scattering geometry, the Thomson scattering regime is characterized by the scattering parameter α that is proportional to the ratio of the x-ray probe scale-length to the plasma screening length λs, where $\alpha=1/k\lambda s$.

Of interest to this study, $\alpha > 1$ results in collective scattering and the plasmon frequency shift from E_0 is determined by the plasmon dispersion relation and the width is determined by Landau damping and collisional damping processes. The shift can be approximated for small values of k using an inversion of Fermi integrals given by Zimmerman [21] that results in a modified Bohm-Gross dispersion relation [21,22],

$$\omega_{pl}^2 = \omega_p^2 + 3k^2 v_{th}^2 \left(1 + 0.088 n_e \Lambda_e^3\right) + \left(\frac{\hbar k^2}{2m_e}\right)^2 \tag{4}$$

where ω_p is the plasma frequency, v_{th} is the thermal velocity, and Λ_{th} is the thermal wavelength.

B. VISAR

Velocity measurements are an important diagnostic capability in many dynamic compression experiments. Wave velocity measurements yield information for material properties under extreme conditions as well as offer relevant platforms to characterize laser-driven shock waves. VISAR is an optical surface measuring technique that can resolve the velocities of a spatial region of a fast-moving object. When coherent light is reflected from a moving surface, the reflected light from the surface is shifted in wavelength with respect to a reference beam of the same wavelength. Interference from the two laser beams generates fringes that can be time resolved via a streak detector (figure 1).

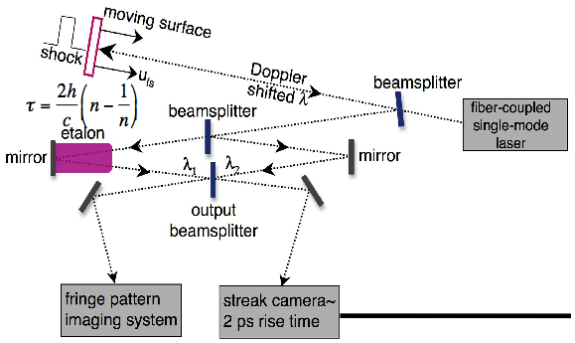

FIG. 1. (Color online). A schematic view of the VISAR system at the MEC end station demonstrating one arm of the interferometry system. A 532 nm probe laser is reflected from the surface of a moving target, after which it will pass through collection optics and be routed into two interferometer stages. Each interferometer is arranged in a Mach-Zender configuration where an etalon of knows thickness is placed into one of the optical beam paths to act as a delay.

Velocity measurements can be accurately determined by the number of whole and partial fringe shifts that occur as the shocked material accelerates past the material surface [23]. A continuous velocity history for all the points that are visible in the image can be made by monitoring the shift and the point at which the surface loses its reflectivity (i.e. shock breakout).

II. EXPERIMENT

A. Seeded x-ray beam

In this study, we employed a seeded LCLS x-ray laser beam to achieve a narrow bandwidth and high-energy resolution that is sufficient enough to observe plasmon resonances. The results from figure 2 will show that the resolution of a SASE beam cannot meet this objective.

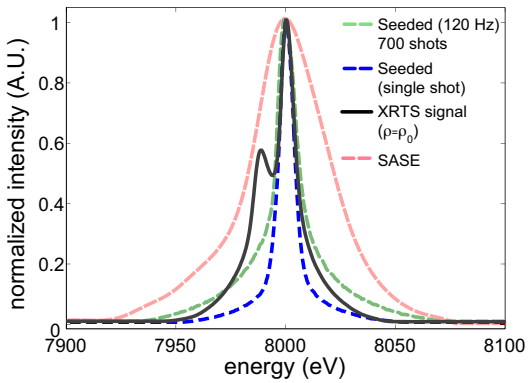

FIG. 2. (Color online). X-ray scattering spectrum of the LCLS beam collected with a 40 μm thick HAPG crystal spectrometer in Von-Hamos geometry for a.) single shot seeded mode; b.) 120 Hz seeded burst mode; c.) SASE mode. A theoretical spectrum of a plasmon (black solid line) at solid-density conditions is plotted using a single shot source spectrum.

In these experiments, the Linac accelerates electrons with a single bunch charge of 150 pC with peak current of 2.91 kA to approximately 13.6 GeV electron beam energy. Within the first 15 undulators the Linac produces Self Amplified Spontaneous Emission (SASE) with about 1 GW power at a wavelength of 1.5 Å, at 8 keV x-ray energy. The electron beam is then passed through a 4-m long chicane while the x-ray beam passes through a diamond crystal that Bragg reflects a narrow energy range of x rays with a bandwidth of $\Delta E/E$ = 0.5 - 1 x 10^{-4} in the center of the broad SASE spectrum. The beating within the transmitted x-ray spectrum creates a 5 MW trailing monochromatic seed pulse about 20 fs or 6 μm behind the broad bandwidth SASE pulse [24]. The electron bunch is delayed slightly, superimposed with the seed pulse and amplified to 10-15 GW in the subsequent 17 undulators before the beam dump separates the electrons from the x-rays, at which point the remaining x-ray beam is transported to the MEC end station resulting in a 20 fs - 50 fs, 1 eV bandwidth coherent x-ray light source. A Be lens is available before a vacuum pumped target chamber to focus the beam to the target chamber center. In this study, the beam is focused to a diameter of 10 μm.

B. Experimental setup

Isochorically heated aluminum

The configuration and the target geometry for this experiment can be demonstrated in figure 3. The target consists of a 25 μm thick aluminum foil irradiated with a narrow bandwidth seeded x-ray laser beam at 120 Hz. In this study the target was moving from left to right during a 1sec exposure cycle so that each x-ray pulse interacts with a fresh target surface. The first portion of a single x-ray pulse isochorically heats the target and the tail end of the same pulse scatters from the heated target. In these experiments, the scattering spectrum was obtained by summing over 100 to 700 x-ray pulses within several minutes.

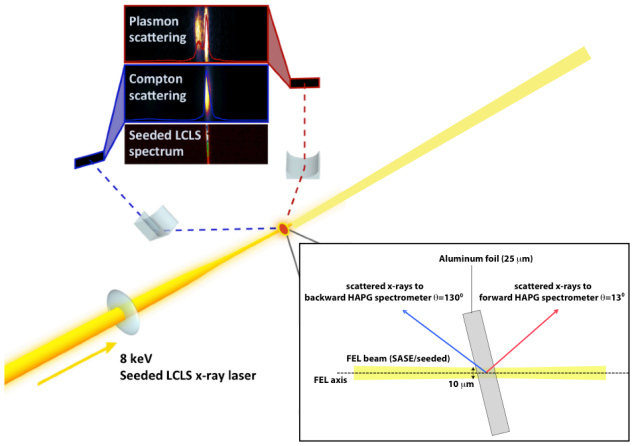

FIG. 3. (Color online). A schematic of LCLS x-ray scattering experiment on solid aluminum is shown together with a target image, the incident LCLS spectrum, x-ray scattering spectra in forward and backward geometry.

To maximize the collection fraction, the x-ray scattering experiments require spectrometers with efficiency of > 0.01 and a high resolving power of $\Delta E/E < 10^{-3}$. In the multi-keV x-ray regime, artificial crystals from low-Z materials such as HAPG (Highly Annealed Pyrolytic Graphite) with a mosaic spread of ~0.1˚ approach these requirements [25 – 27]. To further improve collection efficiency, the distances from the crystal to both the source and the detector are typically chosen to be the same, resulting in mosaic focusing and high spectral resolution [10,28]. In addition, a cylindrically bent crystal in von-Hamos geometry was used to further optimize collection [26].

Measuring Mbar shock waves with VISAR

In our experiment, a single 527 nm square 3 ns pulse with a total laser energy of 6 J, was focused on to CH coated 10 μm /20 μm thick Al step foils in order to generate a laser-driven shock wave that propagates in the direction of the step (figure 4). Using a distributed phase plate, focusing to a 50 μm spot size, a total drive intensity of 35 TW/cm^2 was deposited on the flat CH coated (2 μm thick) portion of the target in order to drive a high pressure shock wave towards the step side of the target.

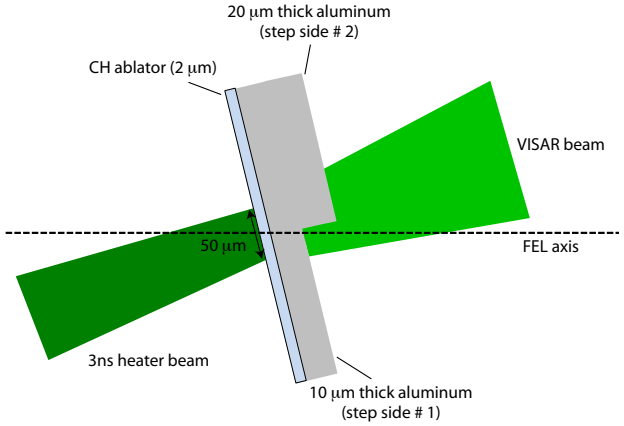

FIG. 4. (Color online). Side view of the VISAR step targets used in this study. The target consists of a CH ablator (laser-drive side) and an aluminum step (VISAR side) that has been precisely machined and measured. A single 6 J 3ns-laser beam is incident on the ablator side, thereby driving a shock towards the step. The

shock breakout can be measured at the two different surfaces on the back side of the step foil and used to infer the shock velocity through the target.

Measurements the shock breakout time are made by the sudden decrease in surface reflectivity when the shock wave reaches the back surface of both the 10 μm thick portion of the target and the 20 μm thick side of the target respectively. Using a known step distance of 10 μm, an absolute velocity can be inferred from the time difference between the two propagation times along the step direction. Moreover, fringe shifts on both detectors with sensitivities of 9.8 km/sec/fringe (streak camera 1), and 1.7 km/sec/fringe (streak camera 2) can be used to unambiguously extract the free surface velocity and therefore infer pressure and compression. Since aluminum has a well-known Hugoniot curve for shock compression [29,30], measurements of the shock velocity in combination with the free surface velocity can be used to accurately determine the stress state at the time of breakout.

III. RESULTS

Figure 5 shows the experimental scattering spectra from solid-density aluminum. Results are shown from the forward scattering and backward scattering spectrometers with the x-ray beam in seeded (figure 5a) and SASE mode of operation (figure 5b). The seeded x-ray beam provides a bandwidth of 1 eV and combined with 8 eV spectrometer resolution resolves the plasmon that is down-shifted from the elastic 8 keV scattering feature by 19 eV.

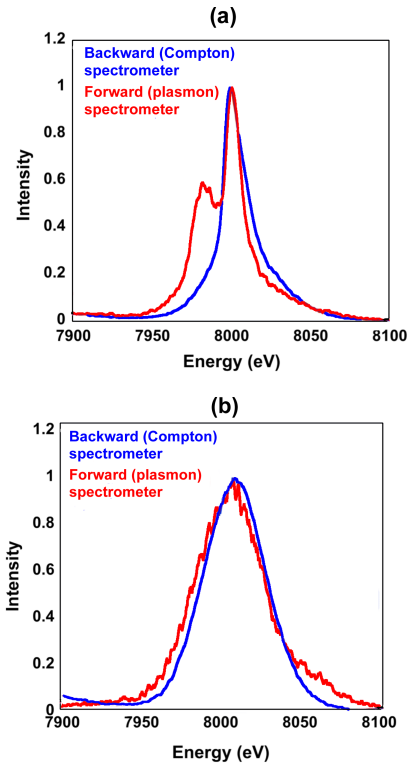

FIG 5. X-ray Thomson scattering data from solid density aluminum targets are shown from forward (plasmon) scattering and backscattering spectrometers for (a) seeded and (b) SASE x-ray beam operation. These data are accumulated over 700 shots at 120 Hz.

The figure also shows the results of the backward scattering spectrometer which observes elastic scattering at 8 keV reflecting the instrument function of the spectrometer convolved with a Gaussian profile that accounts for the statistical fluctuations of the x-ray energy of a seeded beam over 700 shots. The backward spectrometer also measured a Compton scattering feature downshifted in energy by 250 eV (not shown). Here, we note that the plasmon resonance is only observed in forward scattering providing strong evidence of a collective phenomenon as predicted for these conditions; bound-free scattering features are predicted to be negligible in this energy range and no feature has been observed with the Compton spectrometer. For these measurements, the crystal in the forward scattering spectrometer is 40 μm thick while in backscattering we employed a 100 μm thick crystal giving rise to slightly different instrument functions and consequently slight differences in the spectral shape of the elastic scattering feature.

Here, the plasmon frequency is very sensitive to the electron density, but the temperatures are too small to affect the plasmon. The accuracy of the electron density measurement is very high due to the sensitivity of the plasmon resonance to the plasma frequency. Assuming ionization state of Z=3, the measured electron density provides $\rho = 2.7$ g cm^{-3} as expected for solid aluminum. Further analysis is needed to extract the temperature of the plasmon via detailed balance. However, the ions are expected to have temperatures less than 0.1 eV consistent with the observation of Debye-Scherrer rings [31] during the experiment (not shown).

The results from figure 6 illustrate the use of VISAR diagnostic capabilities to measure shock breakout along the vertical direction of the stepped aluminum target. Figure 6b shows the reflectivity drop at the breakout and the free surface expansion of the aluminum surface. The early gradual shift before breakout is indicative of laser preheating in the order of T=0.25 eV that contributes to the shock characteristics. The total transit time for the shock break out at the two different points over the 10 μm step is 0.52 ns +/- 0.05 ns. Thus a shock wave velocity of 19.23 +/- 1.75 km/sec can be inferred resulting in a maximum calculated shock pressure of 3 Mbar, with a material compression of ρ/ρ_o=2.

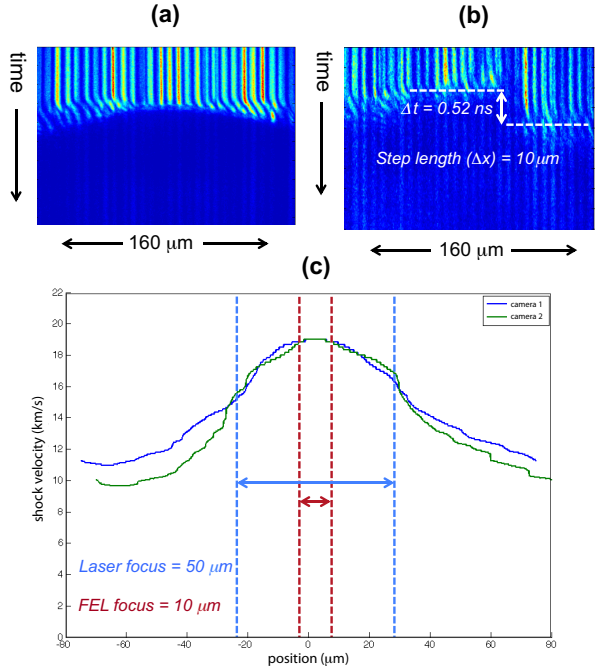

FIG. 6. (a) Shock breakout measurements on a 25 μm thick CH coated planer foil; (b) VISAR results from the 10 μm/20 μm step target configuration described in figure 4; (c) The shock profile inferred from (a), were the maximum velocity is calculated by data recorded from the step targets observed in (b).

Separately, figure 6c demonstrates VISAR measurements from flat, 25 μm thick, aluminum foils that were used to observe the entire shock velocity as a function of the horizontal distance along the laser focus. The results demonstrate a shock profile with a curvature that spans 160 μm along the lateral dimension, however, within +/- 10 μm of the focal center of the drive-laser, the results will show a shock that is near planar at the breakout surface (25 μm). The results indicate that future experiments that use FEL spot sizes of less than 20 μm will be sufficient in investigating planar Mbar shocks that are focused with 50 μm phase plates at propagation lengths of at least 25 μm.

IV. SUMMARY

Accurate measurements of plasmons in isochorically heated aluminum, using the seeded LCLS x-ray beam, have been demonstrated. Taking advantage of the 1 eV spectral bandwidth, an ultra-fast LCLS x-ray beam in combination with high-resolution HAPG crystals can be used to resolve a plasmon shift of 19 eV in x-ray self heated aluminum foils. The resulting energy shift corresponds to an electron density $n_e = 1.8 \times 10^{23} \pm 5\%$. This density is consistent with Z=3 in solid aluminum. This technique demonstrates the possibility for Thomson scattering measurements in compressed matter where the plasmon shift is a sensitive function of the free electron density and where the plasmon intensity provides information on temperature. Furthermore, the results from this study show that Mbar shock waves can be achieved, and accurately characterized using the VISAR system at the MEC end station. Shock wave profiles also demonstrate near-planar shocks that are within XFEL focusing capabilities (ω_0 < 20 μm) and can be used as platform to accurately study aluminum at Mbar pressures.

V. AKNOWLEDGMENTS

This work was performed at the Matter at Extreme Conditions (MEC) instrument of LCLS, supported by the DOE Office of Science, Fusion Energy Science under contract No. SF00515. This work was partially supported by DOE Office of Basic Energy Sciences, Materials Sciences and Engineering Division, under Contract DE-AC02-76SF00515. UZ is grateful to the VolkswagenStiftung for his Peter-Paul-Ewald Fellowship.

VI. REFERENCES

[1]F. Coppari et al., Nature Geoscience (2013).
[2]A. M. Lindenberg et al., Phys. Rev. Lett. 84, 111 (2000).
[3]C. Fortmann et al., Phys. Rev. B 86, 174116 (2012).
[4]B. M. Hegelich et al., Nature 441 (2006).
[5]Y. Sentoku et al., Phys. Rev. Lett. 107, 135005 (2011).
[6]J. D. Lindl et al., Physics of Plasmas 11, 339 (2004).
[7]S. H. Glenzer et al., Physics of Plasmas 19, 056318 (2012).
[8]R. Blandford and D. Eichler, Phys. Rep. 154, 1 (1987).
[9]N. L. Kugland, et al., Nature Physics, (2012).
[10]S. H. Glenzer and R. Redmer, Rev. Mod. Phys. 81, 1625 (2009).
[11]P. Emma et al., Nature Photonics 4, 641 - 647 (2010).
[12]S. H. Glenzer. et al., Phys. Rev. Lett. 98, 065002 (2007).
[13]A. L. Kritcher et al., Science 322, 69 (2008).
[14]P. Neumayer et al., Phys. Rev. Lett. 105, 075003 (2010).
[15]T. Döppner et al., High Energy Density Physics 5, 182–186 (2009).
[16]A. L. Kritcher et al. Phys. Rev. Lett. 103, 245004 (2009).
[17]L. B. Fletcher et al., JINST, 8, C11014 (2013).
[18]J. Chihara, J. Phys. F: Met. Phys. 17, 295 (1987).
[19]G. Gregori et al., Phys. Rev. E. 67, 026412 (2003).
[20]G. Gregori et al., Phys. Rev. E. 74, 026402 (2006).
[21]R. Zimmerman, Many-Particle Theory of Highly Excited Semiconductors (Teubner, Leipzig, 1987).
[22]R. Thiele et al., Phys. Rev. E. 78, 026411 (2008).
[23]L.M. Barker et al., J. Appl. Phys., 43, 4669 (1972).
[24]J. Amann et al., Nature Photonics (2012).
[25]U. Zastrau et al., J. Instrumentation 8, (2013) .
[26]H. Legall et al., Proceedings of FEL 2006, BESSY, Berlin, Germany.
[27]U. Zastrau et al., J. Instrumentation 7, (2012) .
[28]A. Pak et al., Rev. Sci. Instrum. 75, 3747 (2004).
[29]M. D. Knudson et al.,J. Appl. Phys. 94, 4420 (2003).
[30]P. M. Cellier et al., J. Appl. Phys. 98, 113529 (2005).
[31]S. Hau-Riege et al., Phys. Rev. Lett. 108, 217402 (2012).